Int. J. Heat Mass Transfer. Vol. 24, No. 4, pp. 597–609, 1981
Printed in Great Britain

0017–9310/81/040597–13 $02.00/0

TRANSIENT AND STEADY BEHAVIOR OF AN OPEN, SYMMETRICALLY-HEATED, FREE CONVECTION LOOP

HAIM H. BAU and K. E. TORRANCE
Sibley School of Mechanical and Aerospace Engineering, Cornell University, Ithaca, NY 14853, U.S.A.

(*Received* 31 *March* 1980 *and in revised form* 27 *August* 1980)

Abstract—Experiments and analyses are reported for an open, free convection loop. The loop is U-shaped with the lower segment heated; the vertical legs are adiabatic and are connected to an isothermal reservoir. The loop is filled with water or a water-saturated porous medium. Experimental results include the starting transients and the friction factors and heat transfer rates at steady state for flow Reynolds numbers from 4 to 1000. Oscillations are observed with the onset of boiling. Single-phase stability analyses confirm the unstable rest states and the stable steady-states observed in the experiments, and reveal a conditional instability of the steady states. Numerical simulations of the starting transients are obtained and are compared with experiment. Results are applicable to geothermal, solar, and industrial open-loop thermosyphons.

NOMENCLATURE

$a, b,$	loop dimensions, Fig. 2;
$a_0,$	length of heater;
$c_p,$	specific heat;
$d,$	tube inside diameter;
$F, H,$	complex functions defined in (16), (24) and (25);
$f,$	friction factor;
$G,$	parameter defined after (13);
$g,$	acceleration of gravity;
$k,$	thermal conductivity of medium within loop;
$L,$	total length of loop;
$M, N,$	parameters defined after (16) and (24);
$m, n, p,$	nondimensional coefficients in (4) and (8);
$Nu, Pr, Ra,$	Nusselt, Prandtl and Rayleigh numbers in (19);
$P,$	pressure;
$Q,$	total heat input to loop;
$q,$	$m^{1/(3-n)}$;
$Re,$	Reynolds number, $= \hat{u}d/\nu_f$;
$r,$	specific heat ratio;
$s,$	coordinate along the loop;
$T,$	temperature;
$\Delta T,$	temperature difference;
$t,$	time;
$u,$	velocity in loop;
$z,$	vertical coordinate in Fig. 2.

Greek symbols

$\beta,$	volume thermal expansion coefficient;
$\gamma,$	a_0/b;
$\theta,$	angle between fluid velocity vector and the vertical;
$\lambda,$	permeability;
$\nu,$	kinematic viscosity;
$\xi,$	coordinate in Fig. 2;
$\rho,$	density;
$\phi,$	volume porosity;
$\omega,$	reduced growth rate of disturbance;
$\omega^*,$	growth rate of disturbance.

Superscripts

$\tilde{}$	disturbance amplitudes;
$\hat{}$	dimensional quantities.

Subscripts

$cr,$	critical value;
$f,$	fluid property;
$0,$	conditions at inlet;
$m,$	solid matrix;
$s,$	steady state.

1. INTRODUCTION

FLUID motion through an open, free convection loop is examined in this paper. Such loops can transfer fluid between two reservoirs at the same elevation by simply heating or cooling the interconnecting duct. Open loops have been used to explain many geohydrothermal phenomena [1]. Free convection loops, in general, are of interest for many technological applications including the production of geothermal energy, solar heaters, emergency reactor-core cooling, and process industries [2–4].

Prior studies have tended to emphasize closed, free convection loops. In a closed loop, fluid is recirculated continuously around a piping network which forms the loop. Aspects which have been examined include the starting transients [5, 6], steady-state performance [7, 8], and stability of the steady-state motion [7–9]. Both experiments and analyses reveal oscillatory flows for heating conditions which are vertically symmetric (i.e. symmetric about a vertical plane) [7, 9] and slightly asymmetric [8]. The oscillations have been explained in terms of a phase lag between the heating process and the generation of the buoyancy force.

Considerably less is known about open, free convection loops. An open loop differs from a closed loop in that all or part of the circulating fluid may be exchanged with an external reservoir. The temperature and pressure of the reservoir are independent of conditions in the loop. The steady-state performance of open loops has been examined for simple geometries both with prescribed wall temperatures along the loop [10–12] and with significant wall conduction effects [13, 14]. The stability of the rest state for loops with symmetric heating from below has been examined and critical Rayleigh numbers found for the onset of motion [14]. The rest state was stable because cooling and friction processes were able to damp motions in the loop.

From the foregoing, it is clear that very little has been done experimentally or theoretically on open, free convection loops to examine the starting transients, steady-state operation, or flow stability. Those topics form the subject of the present paper. An experimental apparatus is employed, as shown in Fig. 1, in which the geometry and heating conditions are symmetric about a vertical plane. Fluid motion may thus initiate in either direction in the loop. The loop is U-shaped; the lower segment is heated uniformly and the vertical legs are adiabatic. The vertical legs are connected to an isothermal reservoir which is open to the atmosphere. A zero pressure difference between inlet and outlet is thus maintained. In general, a pressure difference between inlet and outlet could be maintained externally, but is not considered in the present study. A unique and novel feature of the loop shown in Fig. 1 is that the working medium may be either water or a water-saturated porous medium. In this paper, we shall refer to the two cases as the "water loop" and the "porous loop", respectively. Flow Reynolds numbers range from 4 to 200 (porous loop) and 100 to 1000 (water loop). Boiling occurs at the higher Re-values in each loop. Results show that the steady states do not oscillate with symmetric heating (in contrast with closed loops), but that boiling leads to oscillations. The experimental results are compared with theoretical descriptions of the transient and steady-states, and with stability analyses of the quiescent and steady-states.

2. EXPERIMENTAL APPARATUS

A schematic diagram of the free convection loop used for the experiments is shown in Fig. 1. The loop is in the form of a vertical U. The loop consists of three straight segments and two ells (70 mm radius of curvature) of pyrex glass tubing (25 mm I.D.; 37 mm O.D.). Each vertical leg is connected at the top to a 30 l. tank. The tanks are interconnected by piping of low resistance ($< 5\%$ of loop resistance) and are cooled by passing tap water through copper cooling coils.

Heating is accomplished by wrapping the lower

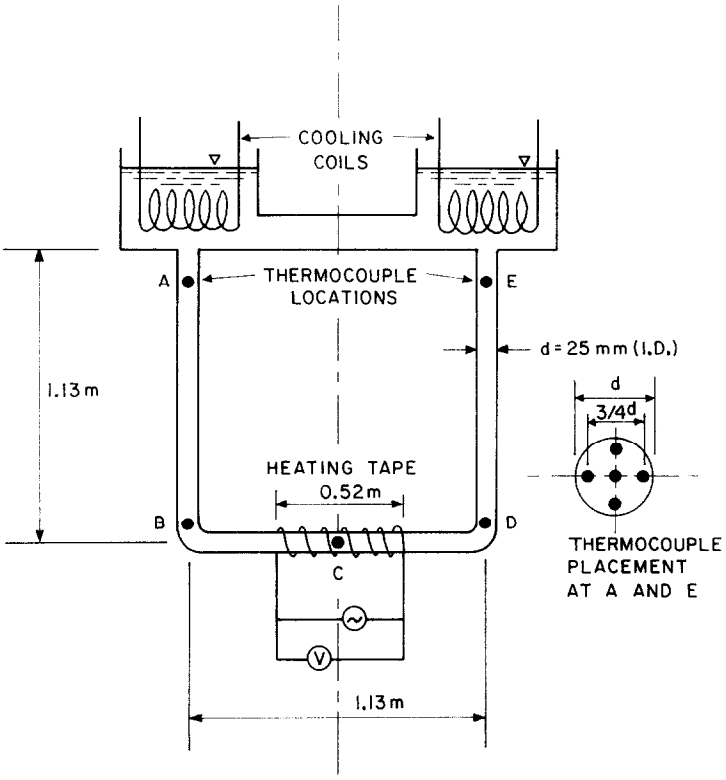

FIG. 1. The experimental apparatus.

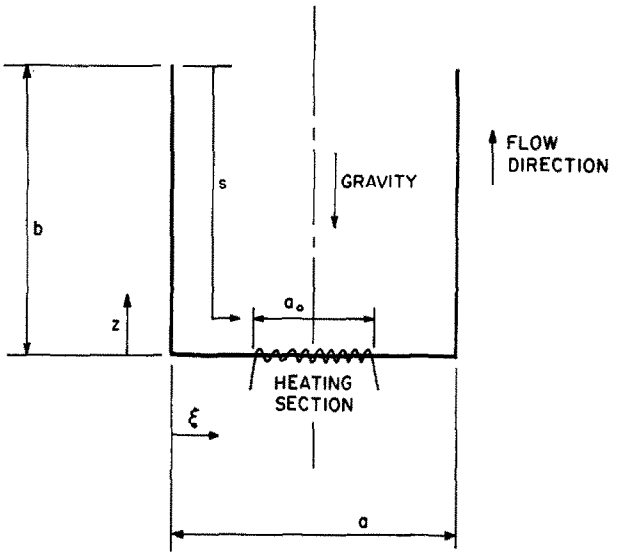

FIG. 2. Geometry and coordinate system.

horizontal leg of the loop with nichrome heating tape. The heating is distributed uniformly over the length shown in Fig. 1. The U-shaped loop is insulated with a layer of foil-covered fiberglass insulation. The input heat flux ranges from 0 to 2300 W and is obtained by measuring the heater resistance and the voltage input from a variable transformer. Heat losses through the insulation are subtracted to obtain the heat inputs reported in this paper.

Temperatures were obtained with 36 gage copper–constantan thermocouples located at stations A–E in Fig. 1. At stations A and E five thermocouples, connected in series and supported over the cross section as shown in Fig. 1, are used to obtain an average fluid temperature. Additional single thermocouples are located along the loop (as shown) and in the tanks at the top.

Experiments are conducted either with distilled water in the loop and tanks, or with a non-fluidizing porous medium in the loop. In the latter case, the loop and tanks are also filled with distilled water. The porous medium consists of closely-packed, uniformly-sized, 5 mm pyrex beads.

Flow rates in the loop are inferred from the corrected input heat flux and the temperature difference between stations E and A (Fig. 1). During the experiments, the reservoirs at the top were found to remain isothermal with essentially no elevation difference between their free surfaces.

3. MATHEMATICAL MODEL

A simple, theoretical model of the experimental loop is formulated in this section. The model is based on the geometry and coordinate system sketched in Fig. 2. The model loop consists of three straight tubes of internal diameter d and is of height b, width a, and overall length L. Following prior work [5–7, 9], one-dimensional, time-dependent balances of mass, momentum, and energy are employed. Properties are assumed constant except for density in the buoyancy term (the Boussinesq approximation). The equations are written in a form suitable for a loop filled with water or a water-saturated porous medium. The velocities and temperatures appearing in the balances are cross-sectionally averaged values.

For an incompressible fluid, the continuity equation implies that the velocity ($\hat{u}$) is constant within the loop and a function only of time ($\hat{t}$)

$$\hat{u} = \hat{u}(\hat{t}). \tag{1}$$

Carets denote the dimensional form of variables which will later be made nondimensional. A momentum balance at any axial station $\hat{s}$ along the loop yields

$$\frac{1}{\phi}\frac{d\hat{u}}{d\hat{t}} + f\frac{\hat{u}^2}{2d} + g(1-\beta_f(\hat{T}-T_0))\cos\theta = -\frac{1}{\rho_f}\frac{\partial P}{\partial \hat{s}} \tag{2}$$

where the various terms are respectively due to inertia, friction, body, and pressure forces. In (2), ϕ is the volume porosity, f is the friction factor, $\hat{T}(\hat{s})$ is the mean fluid temperature at station $\hat{s}$, θ is the angle between the fluid velocity vector and the vertical, and ρ_f is the fluid density at temperature T_0 (the inlet temperature). Integration of (2) from inlet to outlet along the loop yields an integral force balance on the fluid in the loop,

$$\frac{1}{\phi}\frac{d\hat{u}}{d\hat{t}} + f\frac{\hat{u}^2}{2d} = \frac{g\beta_f}{L}\int_0^L \hat{T}\cos\theta\, d\hat{s}. \tag{3}$$

In writing (2) and (3), it is convenient to introduce a friction factor which may be expressed in terms of

steady-state correlations of the form

$$f = \frac{p}{Re^n} \tag{4}$$

where p and n are constants and the Reynolds number is defined in terms of the mean velocity by $Re = \hat{u}d/\nu_f$, where ν_f is the kinematic viscosity of water. For the case of isothermal laminar flow in a straight pipe, we have $p = 64$ and $n = 1$ [15]; for turbulent flow, we have $p = 0.316$ and $n = 0.25$ [15]; and for flow through a porous medium, we have $p = 2d^2/\lambda$ and $n = 1$, where λ is the formation permeability [16]. The foregoing correlations neglect secondary flows due to curvature or buoyancy. We will later fit (4) to our experimental data and implicitly include such effects.

A local heat balance on the loop, neglecting axial conduction and viscous heating, yields

$$r\frac{\partial \hat{T}}{\partial \hat{t}} + \hat{u}\frac{\partial \hat{T}}{\partial \hat{s}} = \begin{cases} \dfrac{4\hat{Q}}{\pi d^2 a_0 \rho_f c_{pf}} & \text{in the heater} \\ 0 & \text{otherwise} \end{cases} \tag{5}$$

where $\hat{Q}$ is the total heat input to the loop and r is a ratio of volumetric heat capacities given by

$$r = \frac{\phi\rho_f c_{pf} + (1-\phi)\rho_m c_{pm}}{\rho_f c_{pf}}. \tag{6}$$

Subscripts f and m respectively denote the fluid and solid matrix appearing in the porous loop. For the porous loop, $\phi = 0.44$ and $r = 0.72$. For the water loop, we have $\phi = 1$ and $r = 1$.

We now introduce nondimensional variables

$$s = \frac{\hat{s}}{b}, \qquad t = \left(\frac{8Q}{\pi}\right)^{1/3}\frac{\nu_f}{bd}\hat{t},$$
$$u = \left(\frac{\pi}{8Q}\right)^{1/3}\frac{d}{\nu_f}\hat{u},$$
$$T = \frac{1}{2}\left(\frac{\pi}{Q}\right)^{2/3}\frac{b}{L}\frac{g\beta_f d^3}{\nu_f^2}(\hat{T} - T_0), \tag{7}$$

$$Q = \frac{b}{L}\frac{g\beta_f d^2}{\rho_f c_{pf}\nu_f^3}\hat{Q}.$$

In addition, the friction factor assumes the form

$$f = \frac{m}{u^n} \quad \text{where} \quad m = p\left(\frac{\pi}{8Q}\right)^{n/3}. \tag{8}$$

Substitution of the foregoing expressions into the momentum and energy equations leads to

$$\left(\frac{2d}{\phi b}\right)\frac{du}{dt} + mu^{2-n} = \int_0^{L/b} T\cos\theta\, ds \tag{9}$$

$$r\frac{\partial T}{\partial t} + u\frac{\partial T}{\partial s} = \begin{cases} 1/\gamma & \text{in the heater} \\ 0 & \text{otherwise} \end{cases} \tag{10}$$

where three geometric parameters from the loop appear: d/b, L/b, and $\gamma \equiv a_0/b$. The steady-state solution (subscript s) is readily obtained as

$$u_s = m^{-1/3-n} \tag{11}$$

$$T_s = \begin{cases} 0 & \text{before the heater} \\ \dfrac{1}{\gamma}m^{1/3-n}(s - s_0) & \text{in the heater} \\ m^{1/3-n} & \text{after the heater} \end{cases} \tag{12}$$

where s_0 is the s-value at the start of the heating section. Without loss of generality in the subsequent stability analyses we shall assume that the heat addition to the horizontal leg is uniformly distributed over its entire length. For the stability analyses, the parameter γ then becomes identical with the aspect ratio of the loop, $\gamma = a_0/b = a/b$.

4. RESULTS AND DISCUSSION

Experimental observations on the transient and steady behavior of the free convection loop are presented in this section. The behavior is compared with results derived from the theoretical model, as appropriate. The discussion is organized in terms of the stability of the rest state (Section 4.1), the transients following the onset of motion (Section 4.2), the steady-state behavior (Sections 4.3 and 4.4), and the onset of boiling (Section 4.5).

4.1. *Onset of motion from a rest state*

Experiments were initiated after allowing the entire system to come into equilibrium with the room. A small amount of heating was then applied to the loop. In all cases, a temperature difference eventually developed between inlet and outlet, indicating a unidirectional flow through the loop. Flows developed in either direction through the loop with essentially equal probability.

The experiments thus suggest that the quiescent initial state (the rest state) is unstable when heated from below. Note that three possible states exist following the application of heating: a quiescent state with no motion ($u = 0$); a pair of circulating flows which are symmetric about the plane of symmetry (with upflow and downflow in each vertical leg); and a state with unidirectional flow through the loop. Only the latter state appeared in the experiments.

We next examine the stability of the rest state to small disturbances. Our objective is to determine if there are any critical conditions associated with the growth of a small disturbance, which then leads to a unidirectional flow through the loop. We first generalize the rest state to include steady heat addition from below but no flow (i.e. $Q \neq 0$ and $u = 0$). The equations governing the rest state and any disturbances are the force balance (9) and a modified energy equation which includes axial heat conduction. For the rest state, axial conduction is the only mechanism available to transfer heat from the heated section to the cooled reservoirs. The modified energy equation is

$$r\frac{\partial T}{\partial t}+u\frac{\partial T}{\partial s}=G\frac{\partial^2 T}{\partial s^2}+\begin{cases}\dfrac{1}{\gamma} & \text{in the heater}\\ 0 & \text{otherwise}\end{cases} \tag{13}$$

where $G=2(\pi/Q)^{1/3}(\pi dk/\rho_f c_{pf} v_f b)$ and k is the thermal conductivity of the fluid or the fluid-saturated porous medium. The conduction solution for the rest state is found from (13) by setting $u=0$:

$$T_s=\begin{cases}\dfrac{1}{2G}(1-z) & \text{in the vertical legs}\\ \dfrac{1}{2G}\left(-\dfrac{1}{\gamma}\xi^2+\xi+1\right) & \text{in the heater.}\end{cases} \tag{14}$$

The coordinates are as shown in Fig. 2. The boundary conditions for (14) are $T_s=0$ at the tops of the vertical legs.

A small perturbation of the rest state is now introduced, of the form

$$u=\varepsilon\tilde{u}e^{\omega^* t} \quad \text{and} \quad T=T_s+\varepsilon\tilde{T}(s)e^{\omega^* t}, \tag{15}$$

where ε is a small quantity, $\tilde{u}$ and $\tilde{T}(s)$ are the amplitudes of the velocity and temperature disturbances, and ω^* is the growth rate. We will consider the system unstable if ω^* has a positive real part.

Following conventional procedures, (15) is substituted into (13), the rest state solution (14) subtracted, and terms of $O(\varepsilon)^2$ neglected. The resulting linearized energy equation for the perturbation temperature $\tilde{T}$may then be integrated, and the resulting $\tilde{T}$ substituted into the buoyancy integral in (9). A characteristic equation for the reduced frequency $\omega=r\omega^*/G$ results:

$$F(\omega)=M+\frac{N}{\omega}-\frac{1}{\omega^2}-\frac{1}{\omega^{5/2}}\frac{(1-\cosh\sqrt{\omega})\sinh\sqrt{\omega}}{\cosh 2\sqrt{\omega}}=0 \tag{16}$$

where $M=2dG^3/\phi br$ and $N=mG^2$. In deriving (16), we assume a laminar friction law of the form $f=m/u$ (i.e. $n=1$) and boundary conditions on $\tilde{T}$of zero at the inlet and zero gradient at the outlet. For simplicity, we assume that the perturbation temperature varies linearly across the heating section (true for short heaters). Using the Nyquist criterion, which will be described in greater detail in Section 4.4, it may be shown that (16) always possesses at least one solution for ω with a positive real part (further details are available in reference [17]). Thus, all rest states are unstable.

The instability of the rest state is in accord with physical reasoning. The vertical legs of the loop are adiabatic. Any asymmetric thermal disturbance in the legs leads to a net buoyancy force. The result is an induced flow with ascending motion in one leg and descending motion in the other. Since the ascending flow is warm (from the heated section) and the descending flow cool (from the cold reservoir), the motion accelerates until buoyancy and friction forces are in balance. Since small disturbances inevitably arise in the experiments, the heated rest states will always undergo a transition to motion. The linear theory reveals that there are no critical conditions required for this transition to occur.

The foregoing unconditional instability of the rest state is in contrast with earlier work on symmetrically-heated open loops in which the vertical legs were not adiabatic [14]. In those loops, heating and cooling processes in the vertical legs provided a mechanism to damp thermal disturbances. Consequently, critical Rayleigh numbers appeared for the onset of fluid motion. Since there is no thermal damping in the vertical legs of the present experiments a critical Rayleigh number does not appear.

4.2. *Starting transients*

Starting transients in the loop were observed experimentally and were simulated numerically. Results for the porous loop are shown in Figs. 3–5; results for the water loop are given in Figs. 6 and 7. The experimental results (Figs. 3 and 6) display the temperature difference between outlet and inlet, $\Delta T_{EA}=T_E-T_A$, and the temperature difference between the center of the heater and the inlet, $\Delta T_{CA}=T_C-T_A$. The calculated results display these variables as well as temperature distributions within the loop (Fig. 5).

Numerical solutions were obtained by approximating (9) and (10) with finite differences. Forward time and backward space differences were used for (10), allowing the fluid temperature to be advanced explicitly in time. The advancement is stable provided the time step satisfies the inequality $u\Delta t/r\Delta s\leq 1$, where Δt is the time step and Δs is the spatial mesh size. The momentum equation (9) is approximated with a backward time difference, steady-state friction factors from Section 4.3, and Simpson's rule for the buoyancy integral. The nonlinear momentum equation is advanced implicitly using the Newton–Raphson technique. The mixed explicit–implicit formulation avoids a severe time step restriction associated with explicit formulations of the momentum equation. Calculations were carried out using the apparatus dimensions shown in Fig. 1.

Truncation errors in the numerical calculations were carefully monitored. The principal error arises from the backward space difference in (10) which creates a numerical diffusion. This false diffusion may be eliminated by setting $u\Delta t/r\Delta s=1$. The laboratory experiments, however, reveal a substantial amount of axial diffusion which is not attributable to heat conduction in the fluid and walls or to heat capacity effects in the walls. The diffusion appears to result from secondary flows in the heated section. The secondary flows are driven by transverse temperature variations within the fluid which, in turn, cause localized natural convection circulations within the duct. The time required to establish these circulations is small compared to the time required to initiate a flow through the

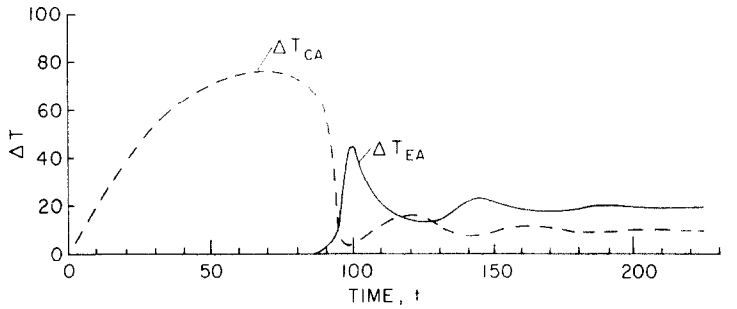

FIG. 3. Experimentally-observed starting transient for the porous loop. The outlet temperature ΔT_{EA} and the heater temperature ΔT_{CA} are shown for $Q = 1.6 \times 10^6$.

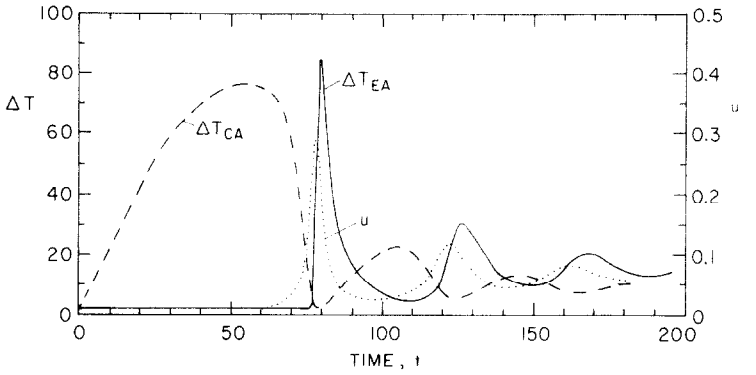

FIG 4. Calculated starting transient for the porous loop. The outlet temperature ΔT_{EA}, the heater temperature ΔT_{CA}, and the flow velocity u are shown for $Q = 1.6 \times 10^6$ and an initiating disturbance of $T_i = 1.75$.

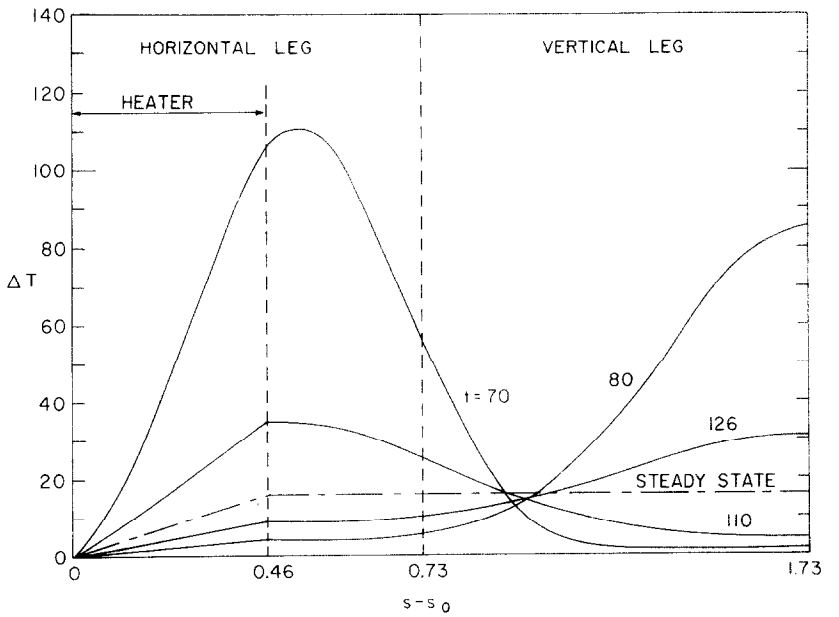

FIG. 5. Calculated temperature distributions within the porous loop at various times t. $Q = 1.6 \times 10^6$ and $T_i = 1.75$.

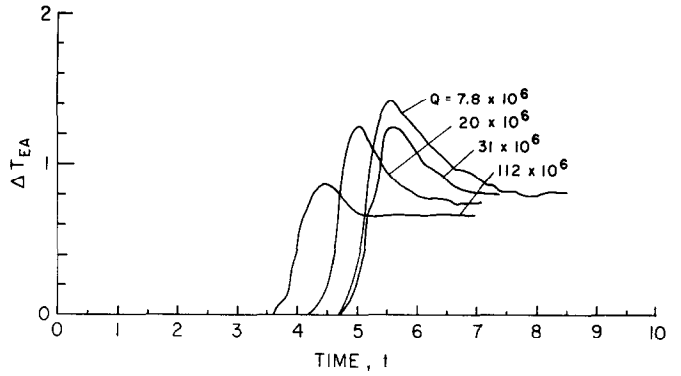

FIG. 6. Experimentally-observed starting transients for the water loop. The outlet temperature ΔT_{EA} is shown for various heating rates Q.

loop. Secondary flows also arise from centrifugal effects in the curved sections of the duct. We find that the effects of the secondary flows may be simulated, at least approximately, by introducing a velocity-dependent numerical diffusion. This is achieved by setting $u\Delta t/r\Delta s = 0.6$ in the calculations for both loops (with $\Delta s = 0.1$). Further details are available in Bau [17]. We note in passing that false diffusion appears to be present, but is not discussed, in the transient calculations of Grief *et al.* [5].

In the experiments as well as the calculations the initial conditions correspond to an isothermal rest state with $T = u = 0$. The inlet temperature is maintained at $T = 0$. Heating is started at $t = 0$. In the experiments, a flow starts after a time period which includes the thermal lag in the heater, the time for secondary flows to diffuse warm fluid to the vertical legs, and the time required to accelerate the fluid in the loop following the appearance of a flow-initiating disturbance. In the calculations, on the other hand, the fluid remained quiescent in the loop unless a flow-initiating disturbance was introduced. Disturbances were thus introduced at $t = 0$ into the calculations by raising the initial temperature of one of the vertical legs from 0 to T_i.

Figures 3 and 4 illustrate experimental and numerical results, respectively, for the porous loop. Clearly, there is a strong qualitative similarity between observed and calculated results. After the start of heating, experimental observations reveal that heat is transferred to the fluid in the horizontal leg by conduction and by local convective circulations. The heater temperature (dashed lines, Figs. 3 and 4) increases during this period. Since the state is unstable, a unidirectional flow through the loop eventually starts; the heater temperature peaks and starts to drop.

Eventually, the outlet temperature in Figs. 3 and 4 increases as warm fluid is discharged. The first peak in ΔT_{EA} corresponds to the initial pulse of warm fluid from the heater. The experimentally-observed peak in ΔT_{EA} is lower than the calculated peak due partly to heat losses and partly to secondary flows in the experiments. The ascending warm pulse accelerates the flow, causing the flow rate, u, in Fig. 4 to increase.

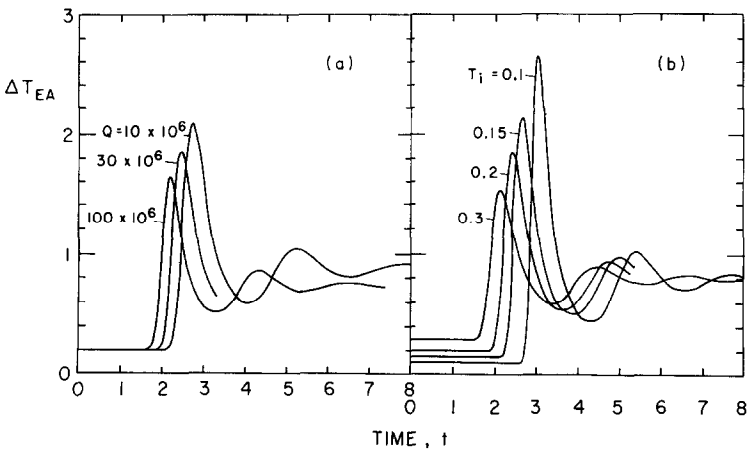

FIG. 7. Calculated starting transients for the water loop. The outlet temperature ΔT_{EA} is shown: (a) for various heating rates Q with the initiating disturbance held fixed at $T_i = 0.2$. (b) For various initiating disturbances T_i with $Q = 30 \times 10^6$.

With the increasing flow rate, cold fluid enters the heater section and leads to the first minimum in ΔT_{CA}. In turn, as this cool fluid starts to rise in the ascending leg, the flow is decelerated. This slowdown allows the heater temperature, ΔT_{CA}, to again increase and peak. The result is an oscillating flow rate, u, and oscillating temperatures. Clearly, the oscillations result from the time lag between the heating process and the subsequent generation of a buoyancy force. Eventually, the oscillations damp out in Figs. 3 and 4 and a steady state is achieved. The migration of the first two warm pulses through the loop is also apparent in the loop temperature distributions shown in Fig. 5. The migration of the first peak is shown by the distributions at $t = 70$ and 80, and the second peak by the distributions at $t = 110$ and 126. The steady state results are also shown, and agree with the analytical solution in (11) and (12).

Figures 6 and 7 illustrate experimental and numerical results, respectively, for the water loop. The general features are similar to those for the porous loop. However, the experimentally-observed temperature oscillations, Fig. 6, are not as well defined as for the porous loop. This is attributed to difficulties in amplifying the experimental signals and to a stronger role for the secondary flows in diffusing the peaks. The time scales for the heating processes in the two loops are quite different. A value of $t = 8$ for the water loop corresponds to 1000 and 410 s, respectively, for the lowest and highest heating rates in Fig. 6. A value of $t = 200$ for the porous loop corresponds to 12 h in Fig. 3.

Comparative calculations for the water loop are shown in Fig. 7. The comparison with the experimental results in Fig. 6 is not as striking as for the porous loop (i.e. Figs. 3 and 4), again as a result of secondary flows. In addition, the experimental results show a longer time delay before the discharge of warm fluid.

The results in Fig. 7 illustrate the influence of the heating rate, Q, and the amplitude of the initiating disturbance, T_i, on ΔT_{EA}. From Fig. 7(a), increasing Q leads to an earlier increase in the outlet temperature and to a reduction in the peak nondimensional outlet temperature. The dimensional temperature, of course, increases with Q. These trends are generally consistent with the experimental transients in Fig. 6. From Fig. 7(b) it is clear that small values of T_i lead to longer time delays and larger peak temperatures. The time delays result because the buoyant acceleration associated with a small disturbance is small. In turn, this leads to a long residence time in the heater and a large peak temperature. Disturbances of $T_i = 0.2$ and 1.75 were used in the calculations for the water and porous loops, respectively.

Figure 7 thus illustrates the influence of Q and T_i on the time delay before the discharge of warm fluid. In the experiments, Fig. 6, the magnitude of the flow-initiating thermal disturbance, T_i, is unknown and in a sense random. The calculations suggest that the experimental time delays may be explained in terms of a systematic influence (Q) and a random influence (T_i).

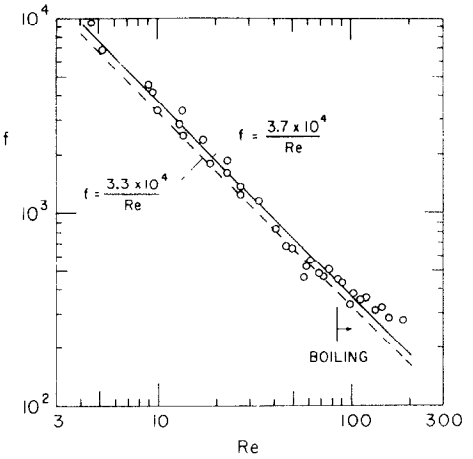

FIG. 8. Friction factor versus Reynolds number for the porous loop (5 mm glass beads). The solid line is the experimental correlation. The dashed line is based on a conventional correlation for the permeability of the porous medium.

4.3. *Steady-state performance*

Following the transients described in the previous section, stable, non-oscillating steady-states were achieved. The friction, flow, and heat-transfer characteristics of the steady states will now be summarized.

The basic experimental data are the outlet–inlet temperature difference, $\Delta \hat{T}_{EA}$ (see Fig. 1), as a function of the heat input to the loop, $\hat{Q}$. The mean velocity in the loop can be deduced from $\Delta \hat{T}_{EA}$ and $\hat{Q}$ by using an overall heat balance [i.e. by integrating (5)]. The result is

$$\hat{u} = \frac{4\hat{Q}}{\pi d^2 \rho_f c_{pf} \Delta \hat{T}_{EA}} \tag{17}$$

Furthermore, the friction factor may be found in terms of these quantities by evaluating the integral in (3) to obtain

$$f = \frac{2dg\beta_f \Delta \hat{T}_{EA} h}{L\hat{u}^2} \tag{18}$$

Friction factors obtained by substituting (17) into (18) are shown in Figs. 8 and 9 for the porous loop and the water loop, respectively. The abscissa is a Reynolds number obtained by using the velocity given by (17). Fluid properties are evaluated by using the mean fluid temperatures at inlet and outlet. The experimental data are seen to scatter about single straight lines. Least-squares fits to the friction factor correlation (4), $f = p/Re^n$, yield the solid lines with the p and n coefficients shown. Some data after the onset of boiling in the porous loop are included ($Re > 85$).

Conventional correlations for f are shown by dashed lines in Figs. 8 and 9. For Fig. 8, a permeability appropriate for closely-packed spheres (the Kozeny–Carman formula [16]) was used. For Fig. 8, the friction factor was based on straight pipes and ells [18]. The differences between the conventional cor-

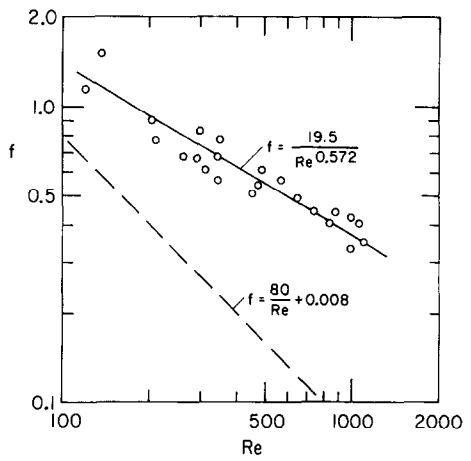

FIG. 9. Friction factor versus Reynolds number for the water loop. The solid line is the experimental correlation. The dashed line is based on a conventional correlation for laminar flow.

relations and our experiments is a result of secondary flows due to curvature and buoyancy. For the porous loop, the differences are relatively small (about 11%). For the water loop, on the other hand, the differences are substantial. This latter fact has been previously noted for a closed free convection loop by Creveling *et al.* [7].

We will now consider an alternative way of presenting the results. We introduce the Rayleigh, Nusselt (following Lapin [10]) and Prandtl numbers, defined by

$$Ra = \frac{g\rho_f c_{pf}\beta_f \Delta\hat{T}_{EA} d^3}{\nu_f k},$$

$$Nu = \frac{\hat{Q}}{dk\Delta\hat{T}_{EA}}, \quad \text{and} \quad Pr = \frac{\rho_f c_{pf}\nu_f}{k}. \tag{19}$$

After rearrangement, and combining with (4), we obtain the friction factor, flow rate, and temperature difference $\Delta\hat{T}_{EA}$ as explicit functions of the independent variable $\hat{Q}$. In nondimensional form, we have

$$f = p^{3/3-n}\left(\frac{\pi}{8Q}\right)^{n/3-n}$$

$$Re = \left(\frac{8Q}{\pi p}\right)^{1/3-n} \tag{20}$$

$$Nu = \frac{\pi}{4} Pr\left(\frac{8Q}{\pi p}\right)^{1/3-n}.$$

If desired, the Rayleigh number may be found from (19) and (7). The result is $Ra = (L/b)\,Pr^2 Q/Nu$. Equations (20) are shown by solid lines in Fig. 10 for the water loop. p and n values from Fig. 9 have been used. The experimental data are also shown.

4.4. *Stability of the steady-state*

Previous work on single-phase (non-boiling) closed loops has revealed a family of oscillatory flows when the heating was symmetric [8]. The present experiments, however, indicate that non-oscillatory steady-states exist for both the porous and water loops before the onset of boiling. To see if these observations are valid in general, we next carry out a stability analysis of the steady flows.

We first introduce a small perturbation of the steady-state of the form

$$u = u_s + \varepsilon\tilde{u}e^{\omega^* t} \quad \text{and} \quad \tilde{T} = T_s + \varepsilon\tilde{T}(s)e^{\omega^* t}. \tag{21}$$

Again, we will consider the system unstable if the growth rate ω^* has a positive real part. We proceed by substituting (21) into the governing equations (9) and (10) and subtracting the steady-state solution (11) and (12). Neglecting terms of $O(\varepsilon^2)$ we have the linearized equations

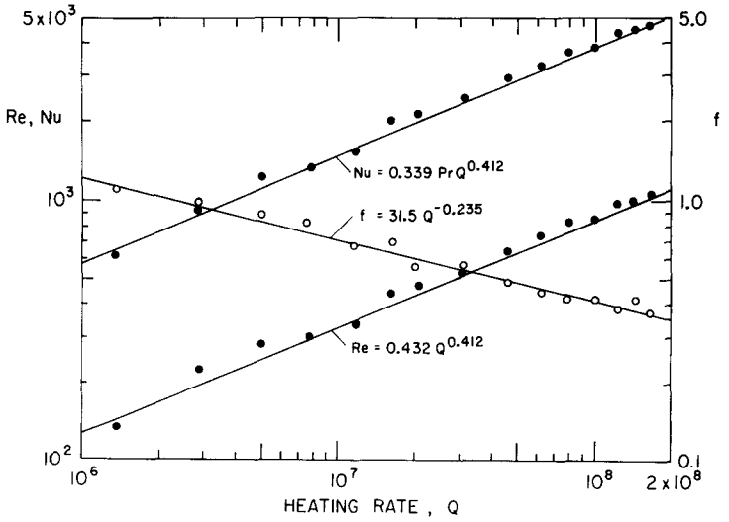

FIG. 10. Friction factor f, Reynolds number Re, and the Nusselt number Nu as functions of the nondimensional heating rate Q for the water loop. The solid lines are the indicated theoretical correlations from (20).

$$r\omega^* \tilde{T} + u_s \frac{\partial \tilde{T}}{\partial s} + \tilde{u} \frac{\partial T_s}{\partial s} = 0$$

(22)

$$\tilde{u}\left[\frac{2d}{\phi b}\omega^* + m(2-n)u_s^{1-n}\right] = \int_0^{L,b} \tilde{T}\cos\theta \, ds.$$

Integration of the energy equation yields

$$\tilde{T} = \begin{cases} 0 & \text{in the descending leg} \\ \dfrac{q}{\gamma r\omega^*}\tilde{u}(e^{-qr\omega^* s} - 1) & \text{in the heater} \\ \dfrac{q}{\gamma r\omega^*}\tilde{u}(e^{-q\gamma r\omega^*} - 1)e^{-qr\omega^* z} & \text{in the ascending leg} \end{cases} \quad (23)$$

where $q = m^{1/3-n}$. Coordinates are as shown in Fig. 2 and the inlet boundary condition $\tilde{T} = 0$ has been employed.

After evaluating the integral in the momentum equation in (22), a characteristic equation for the reduced frequency results

$$F(\omega) = M + \frac{N}{\omega} + \frac{1}{\omega^3}(1 - e^{-i\omega})(1 - e^{-\omega}) = 0$$

(24)

where $\omega = qr\omega^*$, $M = 2d\gamma/\phi brq^3$, and $N = \gamma(2-n)$. We will use the Nyquist criterion [19] to help in the search for roots of (24) which possess positive real parts. Consider first the closed curve shown in Fig. 11(a). Consider next the complex plane defined by

$$H(\omega) = F(\omega) - M \quad (25)$$

which is shown in Fig. 11(b). The Nyquist criterion says, in essence, that the number of roots of (24) within a closed curve [as shown in Fig. 11(a)] is equal to the number of times $F(\omega)$ encircles the point $-M$ in the $H(\omega)$ plane as ω traverses the closed curve. It is necessary that $F(\omega)$ be analytic within, and analytic and nonzero on, the closed curve.

To apply the criterion, we map the closed curve in Fig. 11(a) into the H-plane in Fig. 11(b). In addition, to find all roots with a positive real part, we extend the closed curve to include the entire right half of the ω-plane. The extended curve is mapped as follows: The semicircle ABC maps to the origin of the H-plane. The semicircle DEF maps to a half circle at infinity in the right half of the H-plane. The mapping of the positive imaginary axis CD is shown by the solid curves in Fig. 11(b) for four different values of n. The negative imaginary axis FA is mapped by the mirror-image of the solid curves about the real axis. The curves in Fig. 11(b) correspond to $\gamma = 0.46$ (the present experiments).

As stated earlier, in order for $F(\omega)$ to have roots within the closed curve shown in Fig. 11(a), the point

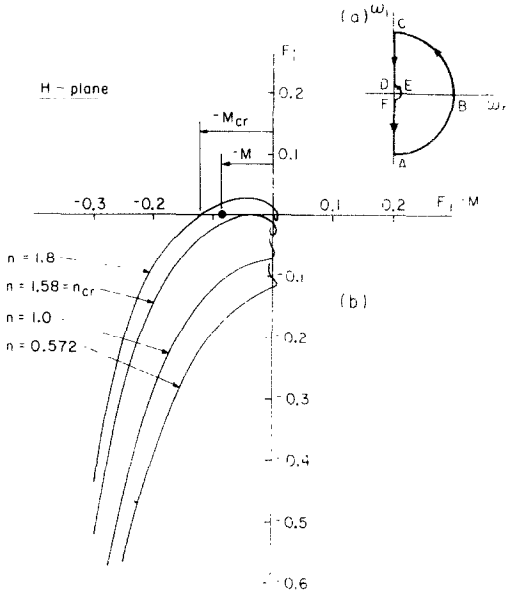

FIG. 11(a). The ω-plane with a closed curve indicating the integration path to be mapped into the H-plane. (b) Nyquist plot of (24) in the complex H-plane defined by (25). The locations of a point $-M$, and a critical value $-M_{cr}$, are shown. The curves correspond to the branch CD in the ω-plane. The curve parameter is the exponent n in (4). $\gamma = 0.46$.

$-M$ in Fig. 11(b) should be encircled by the mapped curve. Note that M is an independent, real parameter which involves geometric factors and the constants m and n from (8). The filled circle in Fig. 11(b) indicates a possible location for the point $-M$. Clearly, there is a critical value n_{cr} [= 1.58 in Fig. 11(b)] at which the mapped curve is tangent to the real axis. For $n < n_{cr}$, the mapped curve never crosses the real axis. Since a point $-M$ can never be encircled, the system is unconditionally stable. For $n > n_{cr}$, the mapped curve crosses the real axis and may encircle a point $-M$ as shown for $n = 1.8$. The system is thus unstable for a range of values $0 < M < M_{cr}$, where M_{cr} varies with n.

The value of n_{cr} varies with γ as shown in Fig. 12. For $n < n_{cr}$ the steady state flows are unconditionally stable. For $n > n_{cr}$ the flows are unstable if $0 < M < M_{cr}$ and stable if $M > M_{cr}$. This is a zone of conditional stability. Note that the minimum value of n_{cr} is 1.528.

To compare the foregoing stability analyses with our experiments, estimates for n are needed. Note that the experimental friction factors depend explicitly on Q (Fig. 10), and when graphed vs Re (Figs. 8 and 9) best-fit values of $n = 1$ and 0.572 are obtained. On the other hand, the friction factor appearing in the stability analysis is treated as an explicit function of Re with Q held constant. For the case of $Q = 0$, the approximation $n = 1$ is expected to hold (dashed lines in Figs. 8 and 9). Clearly there is uncertainty as to the proper value of n [8], but $n = 1$ appears to be a realistic upper bound. Since this value is below the minimum value of

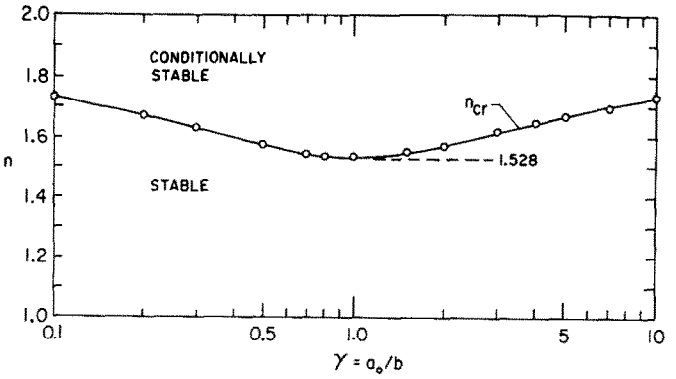

FIG. 12. Critical values of the exponent n in (4) for various values of γ. n-values below and above the solid line correspond, respectively, to stable and conditionally-stable flows.

n_{cr} of 1.528 in Fig. 12, we conclude that the steady-state flows will always be stable. This result is confirmed by our experiments.

4.5. *Onset of boiling*

Boiling was observed in both the porous and the water loops during the starting transients and at steady-state. Boiling during the starting transient is similar in both loops and will be described for the porous loop. Boiling in the porous loop occurred when the input heat flux Q exceeded 2×10^6. Just above this value the heater temperature (see dashed line in Fig. 3 for reference) reached the saturation temperature during the transient. The heater temperature remained at saturation until the induced convective flow quenched the boiling process with an influx of cold water. The heater temperature then dropped below saturation and the remaining transient was similar to the non-boiling case (Fig. 3). For $Q > 25 \times 10^6$ boiling occurred during the transients and at steady-state. Occasionally, the saturation temperature plateau was followed by a short dryout period before quenching took place. At very high values of Q, the dryout process persisted and was not quenched. An example of such a transient is shown in Fig. 13. The linear behavior indicates the absence of convective cooling by flow through the loop. The glass loop ultimately fractured. Dryout was not observed in the water loop.

With the appearance of boiling during the steady-state operation of the loop, the temperature recordings indicated the presence of oscillations. For the water loop, which showed boiling at steady-state for $Q > 110 \times 10^6$, small-amplitude oscillations with a period of 15–20 s appeared in the outlet temperature. The oscillations were nearly periodic as shown in Fig. 14(a) for $Q = 112 \times 10^6$, but the period does not correspond to any obvious characteristic time in the system. Approximately once per hour, a large-

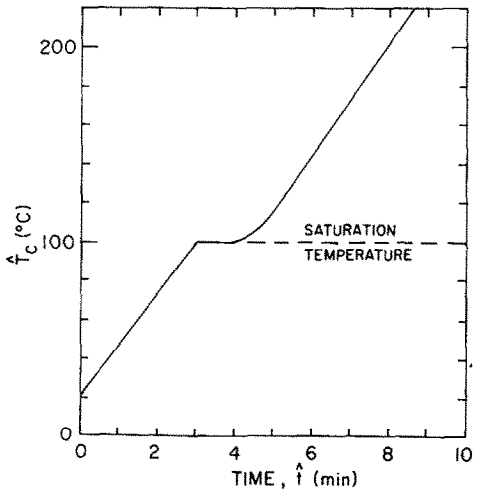

FIG. 13. Starting transient in the porous loop with a heat flux high enough to lead to dryout; $Q = 90 \times 10^6$. T_c is the temperature in the heating section.

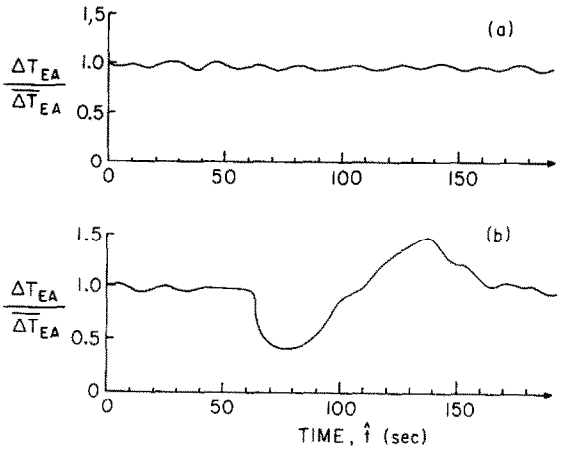

FIG. 14. The outlet temperature ΔT_{EA} in the water loop following the onset of steady-state boiling in the heater, $Q = 112 \times 10^6$. $\overline{\Delta T_{EA}}$ is the mean outlet temperature. (a) Regular oscillations occurring when a large vapor bubble forms in the horizontal heated leg. (b) Strong oscillations associated with the release of the vapor bubble approximately once per hour.

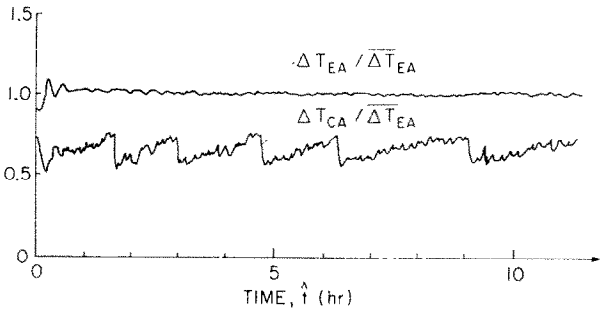

FIG. 15. The outlet temperature ΔT_{EA} and the heater temperature ΔT_{CA} in the porous loop after the onset of steady-state boiling in the heater, $Q = 53 \times 10^6$. $\overline{\Delta T}_{EA}$ is the mean outlet temperature.

amplitude oscillation occurred as shown in Fig. 14(b). The large oscillation is associated with the formation and escape of a large vapor bubble from the heater. The period of the oscillation corresponds to the flow time through the loop. For the porous loop, outlet temperature oscillations also occurred as shown by the upper curve in Fig. 15. Relatively small oscillations result because the porous media restricts bubble motions. (Due to the relative steadiness of the outlet temperature, the inferred friction factors were included in Fig. 8.) The large-amplitude oscillations in the heater temperature (lower curve), are attributed to either a single vapor bubble or to a dispersed vapor zone which restricts flow through the loop. The disappearance of the bubble or the zone leads to a drop in temperature. Reversals of the flow direction in the loop were not observed after the start of boiling; such an event is not precluded, however.

5. CONCLUSIONS

Results from our study of the symmetrically-heated free convection loop sketched in Fig. 1 may be summarized:

1. The rest state is found to be unconditionally unstable when heated. A flow always develops.

2. A time delay in the production of warm discharge fluid always occurs. This is principally due to the time required for secondary flows to diffuse warm fluid to the vertical legs, to the time required for the onset and growth of a flow-initiating disturbance, and to the finite transit times in the loop.

3. Non-oscillating steady states are observed in the absence of boiling. Theory suggests that a pathological friction law could lead to instability.

4. Secondary flows increase the steady-state friction factors above estimates based on conventional correlations. Secondary flows are especially significant for the water loop, but are of small importance in the porous loop.

5. The onset of boiling leads to oscillating flows. Occasional strong oscillations appear and are attributed to the periodic formation and escape of large vapor bubbles in the horizontal heating section.

Acknowledgements—The authors would like to thank Professor D. L. Turcotte for many helpful discussions. This research has been supported by the Division of Engineering of the National Science Foundation under Grant ENG-7823542.

REFERENCES

1. J. W. Elder, Heat and mass transfer in the earth: hydrothermal systems, *Bull. N.Z. Dep. Scient. Ind. Res.* **169**, (1966).
2. D. Japikse, Advances in thermosyphon technology, in *Advances in Heat Transfer*, edited by T. F. Irvine, Jr. and J. P. Hartnett, Vol. 9, pp. 1–111. Academic Press, New York (1973).
3. A. Shitzer, D. Kalmanoviz, Y. Zvirin and G. Grossman, Experiments with a flat plate solar water heating system in thermosyphonic flow, *Solar Energy* **22**, 27–35 (1979).
4. J. L. Gillette, R. M. Singer, J. V. Tokar and J. E. Sullivan, Experimental study of the transition from forced to natural circulation in EBR-II at low power and flow, *J. Heat Transfer* **102**, 525–530 (1980).
5. R. Greif, Y. Zvirin and A. Mertol, The transient and stability behavior of a natural convection loop, *J. Heat Transfer* **101**, 684–688 (1979).
6. C. D. Alstad, H. S. Isbin, N. R. Amundson and J. P. Silvers, Transient behavior of single-phase natural-circulation loop systems, *A.I.Ch.E.Jl* **1**, 417–425 (1955).
7. H. F. Creveling, J. F. de Paz, J. Y. Baladi and R. J. Schoenhals, Stability characteristics of a single-phase free convection loop, *J. Fluid Mech.* **67**, 65–84 (1975).
8. P. S. Damerell and R. J. Schoenhals, Flow in a toroidal thermosyphon with angular displacement of heated and cooled sections, *J. Heat Transfer* **101**, 672–676 (1979).
9. P. Welander, On the oscillatory instability of a differentially heated fluid loop, *J. Fluid Mech.* **29**, 17–30 (1967).
10. Yu. D. Lapin, Heat transfer in communicating channels under conditions of free convection, *Thermal Engng* **16**, 94–97 (1969).
11. J. L. Boy-Marcotte, P. Chevalier and M. Jannot, Study of temperature gradients due to gas thermosyphons induced within the Phenix nuclear reactor, in *Heat Transfer and Turbulent Buoyant Convection*, edited by D. B. Spalding and N. Afghan, Vol. II, pp. 555–565. Hemisphere, New York (1977).
12. K. E. Torrance, Open-loop thermosyphons with geological applications, *J. Heat Transfer* **101**, 677–683 (1979).
13. I. G. Donaldson, The simulation of geothermal systems with a simple convective model, in *U.N. Symp. on the Development and Utilization of Geothermal Resources Pisa*, Vol. 2, pt. 1, pp. 649–654 (1970).
14. K. E. Torrance and V. W. C. Chan, Heat transfer by a free convection loop embedded in a heat-conducting solid, *Int. J. Heat Mass Transfer* **23**, 1091–1097 (1981).

15. E. R. G. Eckert and R. M. Drake, Jr., *Analysis of Heat and Mass Transfer*, p. 370. McGraw-Hill, New York (1972).
16. J. Bear, *Dynamics of Fluids in Porous Media*, pp. 133, 148 and 166. Elsevier, New York (1972).
17. H. H. Bau, Experimental and theoretical studies of natural convection in laboratory-scale models of geothermal systems, Ph.D. Thesis, Cornell University, Ithaca, New York (1980).
18. *Process Pipe Fittings and Hardware*, Corning Glass Works Catalog PFH-3178MA, Corning, New York (1978).
19. G. F. Carrier, M. Krook and C. E. Pearson, *Functions of a Complex Variable—Theory and Techniques*, p. 61. McGraw-Hill, New York (1966).

COMPORTEMENT EN REGIME PERMANENT OU VARIABLE D'UNE BOUCLE OUVERTE, CHAUFFEE SYMETRIQUEMENT EN CONVECTION NATURELLE

Résumé—On rapport des expériences et des analyses sur une boucle ouverte à convection naturelle. La boucle est en forme de U avec le segment inférieur chauffé; les parties verticales sont adiabatiques et sont connectées à un réservoir isotherme. La boucle est remplie d'eau ou d'un milieu poreux satiné d'eau. Des résultats concernent le régime d'initiation, les coefficients de frottement et les flux thermiques transférés en régime permanent pour des nombres de Reynolds entre 4 et 1000. On observe des oscillations avec apparition d'ébullition. Des analyses de stabilité en simple phase confirment les états instables observés expérimentalement et elles révèlent une instabilité conditionnelle des états permanents. Des simulations numériques des régimes variables au départ sont obtenues et elles sont comparées avec l'expérience. Les résultats sont applicables à la géothermie, aux thermosyphons à boucle ouverte solaires et industriels.

INSTATIONÄRES UND STATIONÄRES VERHALTEN EINES OFFENEN, SYMMETRISCH BEHEIZTEN KREISLAUFS BEI FREIER KONVEKTION

Zusammenfassung—Es wird über Experimente und Untersuchungen an einem offenen Kreislauf bei freier Konvektion berichtet. Der Kreislauf hat U-Form, wobei das untere Segment beheizt wird und die mit einem isothermen Reservoir verbundenen Schenkel adiabat sind. Der Kreislauf ist mit Wasser oder einem mit Wasser gesättigten porösen Medium gefüllt.

Die experimentellen Ergebnisse umfassen die Anlaufzustände, die Widerstandsbeiwerte und den Wärmeübergang im stationären Zustand für Reynolds-Zahlen der Strömung von 4 bis 1000. Beim Einsetzen des Siedens werden Oszillationen beobachtet. Stabilitätsuntersuchungen im Bereich der Einphasenströmung bestätigen die instabilen Ruhelagen und die stabilen stationären Zustände, die bei den Experimenten beobachtet wurden, und zeigen eine bedingte Instabilität der stationären Zustände. Es wurden numerische Simulationen der Anlaufzustände durchgeführt und mit den Experimenten verglichen. Die Ergebnisse sind anwendbar auf geothermische, solare und industrielle Thermosyphons des offenen Typs.

НЕСТАЦИОНАРНЫЙ И СТАЦИОНАРНЫЙ РЕЖИМЫ ОТКРЫТОГО СИММЕТРИЧНО НАГРЕВАЕМОГО СВОБОДНО-КОНВЕКТИВНОГО КОНТУРА

Аннотация — Описаны эксперименты и представлен анализ открытого свободно-конвективного *U*-образного контура, нижняя часть которого нагревается, а вертикальные участки адиабатичны и подсоединены к изотермическому резервуару. Контур заполнен водой и пористым веществом. Приведены результаты экспериментального определения параметров начального неустановившегося процесса и коэффициентов трения, а также интенсивностей теплопереноса в стационарном режиме в диапазоне чисел Рейнольдса от 4 до 1000. Колебания наблюдаются при возникновении кипения. С помощью анализа устойчивости для однофазной среды подтверждены экспериментально наблюдаемые неустойчивые состояния покоя и устойчивые стационарные состояния и выявлена условная неустойчивость стационарных состояний. Проведено численное моделирование первоначально неустойчивых состояний и дано сравнение с экспериментом. Результаты можно использовать при анализе геотермальных, солнечных и промышленных термосифонов открытого типа.